ResearchGate

See discussions, stats, and author profiles for this publication at: https://www.researchgate.net/publication/3201881

Multiangle Imaging SptectrRadiometer (MISR) description and experiment overview

Article *in* IEEE Transactions on Geoscience and Remote Sensing · August 1998

DOI: 10.1109/36.700992 · Source: IEEE Xplore

CITATIONS
687

READS
521

16 authors, including:

Ralph Kahn
NASA
450 PUBLICATIONS 19,284 CITATIONS
SEE PROFILE

Roger Davies
University of Auckland
127 PUBLICATIONS 5,206 CITATIONS
SEE PROFILE

Howard Gordon
University of Miami
231 PUBLICATIONS 20,003 CITATIONS
SEE PROFILE

J.-P. Muller
University College London
531 PUBLICATIONS 14,644 CITATIONS
SEE PROFILE

Some of the authors of this publication are also working on these related projects:

Global Mapping of Aerosol Optical & Microphysical Parameters using Machine Learning (AEROMAP) View project

Aerosols and Climate View project

All content following this page was uploaded by J.-P. Muller on 01 November 2012.

The user has requested enhancement of the downloaded file.

Multi-angle Imaging SpectroRadiometer (MISR) Instrument Description and Experiment Overview

David J. Diner, Jewel C. Beckert, Terrence H. Reilly, Carol J. Bruegge, James E. Conel, Ralph A. Kahn, John V. Martonchik
Jet Propulsion Laboratory, California Institute of Technology
Pasadena, CA911 09, USA

Thomas P. Ackerman
Department of Meteorology, Pennsylvania State University
University Park, PA 16802, USA

Roger Davies
Institute of Atmospheric Physics, University of Arizona
Tucson, AZ 85721, USA

Siegfried A. W. Gerstl
Nonproliferation and International Security, Los Alamos National Laboratory
Los Alamos, NM 87545, USA

Howard R. Gordon
Department of Physics, University of Miami
Coral Gables, FL 33124, USA

Jan-Peter Muller
Dept. of Geomatic Engineering, University College London
London, WC 1 E 6BT, United Kingdom

Ranga Myneni
Department of Geography, Boston University
Boston, MA 02215, USA

Piers J. Sellers
Code CB, NASA Johnson Space Center
Houston, TX 77058, USA

Bernard Pinty, Michel M. Verstraete
Space Applications Institute, EC Joint Research Centre
1-21020, Ispra (VA), Italy

Submitted to: *IEEE Transactions on Geoscience and Remote Sensing*
October 1997

Send correspondence to:

David J. Diner
Mail stop 169-237
Jet Propulsion Laboratory
4800 Oak Grove Dr.
Pasadena, CA 91109

Tel.: (818) 354-6319
FAX: (818) 393-4619
djd@jord.jpl.nasa.gov

Abstract--The Multi-angle Imaging SpectroRadiometer (MISR) instrument is scheduled for launch aboard the first of the Earth Observing System (EOS) spacecraft, EOS-AM1. MISR will provide global, radiometrically calibrated, georectified, and co-registered imagery at nine discrete viewing angles and four visible/near-infrared spectral bands. Algorithms developed specifically to capitalize on this measurement strategy will be used to retrieve geophysical products for studies of clouds, aerosols, and surface radiation. This paper provides an overview of the as-built instrument characteristics and the application of MISR to remote sensing of the Earth.

I. INTRODUCTION

The MISR instrument *[1]* was delivered by the Jet Propulsion Laboratory (JPL) to the spacecraft contractor, Lockheed Martin Missiles and Space of Valley Forge, Pennsylvania, on May 26, 1997. This delivery marked one of many major milestones in preparation for launch, currently scheduled for late-June 1998 from Vandenberg Air Force Base in California.

MISR measurements are designed to improve our understanding of the Earth's ecology, environment, and climate. The illumination source for MISR imagery is reflected sunlight. A detailed understanding of how sunlight is scattered in different directions is necessary in order to determine how changes in the amounts, types, and distribution of clouds, airborne particulate, and surface cover affect our climate. MISR takes the novel approach of imaging the Earth in nine different view directions to infer the angular variation of reflected sunlight and the physical characteristics of the observed scenes. MISR'S cameras are arranged with one pointing toward the nadir (designated An), one bank of four pointing in the forward direction (Af, Bf, Cf, and Df in order of increasing off-nadir angle), and one bank of four pointing in the aftward direction (Aa, Ba, Ca, and Da). Each of the nine cameras obtains images at four wavelengths (blue, green, red, and near-infrared). On-board detector-based calibration hardware provides high radiometric accuracy and stability of the data. This observing strategy enables the rigorous use of radiative transfer theory and physically-based models to facilitate the retrieval of cloud, aerosol, and surface properties. Figure I is a rendering of the MISR instrument measurement concept. The EOS-AM I orbit is near-polar, sun-synchronous with a 10:30 a.m. equator crossing time on the descending node, and has a16-day global coverage repeat cycle.

11. INSTRUMENT OVERVIEW

A. *Architecture*

At the heart of the MISR instrument is the optical bench, which holds the cameras at their light-admitting end with the detector end cantilevered into the instrument cavity. The fore-aft cameras are paired in a symmetrical arrangement and set at fixed view angles on the optical bench. In order to acquire images with nominal view angles, relative to the Earth's surface, of 0°, 26.1°, 45.6°,60.0°, and 70.5° for An, Af/Aa, Bf/Ba, Cf/Ca, and Df/Da, respectively, each off-nadir camera is oriented at a fore/aft pointing angle that is somewhat smaller than the corresponding view angle to account for Earth curvature. This along-track mounting angle is called the boresight angle. The convention used is that a positive (negative) boresight angle points the camera forward (aftward). Additionally, to maximize overlap of the swath seen at all angles, the effect of Earth rotation during the 7-minute interval between viewing a point on the surface by the Df and Da cameras must be taken into consideration. This is accomplished by incorporating a slight cross-track offset angle into each camera's view direction. For these angles, the convention is that a positive (negative) offset points the camera in the same (opposite) direction as the Earth is rotating.

The primary support structure provides kinematic attachment of the instrument to the spacecraft bus and is designed to maintain rigid support for the optical bench. Connection of the optical bench to the instrument structure is provided through a system of titanium tubular bipeds. The instrument enclosure provides a structural mount for the nadir-facing radiators. In addition, it houses the system electronics and flight computers, and incorporates external optical baffles to keep specular glints from neighboring instruments from illuminating MISR'S optical calibration surfaces.

A cutaway drawing of the MISR instrument is shown in Figure 2, and a photograph of the instrument on the end bell of the JPL 10-foot thermal vacuum chamber is shown in Figure 3. A summary of its specifications and as-built characteristics is shown in Tables 1, II, and 111. In Table I, the small difference between the as-built power usage and the allocation at delivery has been waived by the EOS-AM 1 project office. Camera pointing angle measurements shown in Table II are relative to the instrument coordinate system. The view angles vary slightly with orbital location and position within each camera's field-of-view; the values in Table II are calculated for the center of the red band field-of-view and the point in the orbit at which the spacecraft is above the equator.

Slight modifications to all of the angles shown will occur when the instrument-to-spacecraft pointing is established. In Table 111, spectral bandwidths are larger than specification due to larger than expected out-of-band spectral response as a result of scattering within the spectral filters. Where required, a correction for this response is incorporated into the data processing algorithms. Further details on the preflight instrument calibration and characterization maybe found in *[2]*.

B. Cameras

The MISR lenses are superachromatic, 7-element refractive f/5.5 telecentric designs. Focal lengths vary with view angle in order to maintain cross-track sample spacing. A double plate Lyot depolarizer is incorporated into each of the cameras in order to render them polarization insensitive. The lenses are mounted in aluminum barrels with some additional materials to accommodate thermally induced dimensional changes of the lenses during flight. Each MISR camera contains a camera head which houses the focal plane structure and to which is attached the driver electronics for the charge-coupled device (CCD) line arrays. The camera heads and electronics are identical for all nine cameras, leading to a modular design in which only the lens barrels are unique.

MISR contains 36 parallel signal chains corresponding to the four spectral bands in each of the nine cameras. Each signal chain contains the output from the 1520 pixels (1S04 photo-active plus 8 light-shielded plus 8 "overclock" samples of the CCD serial register) in each detector array. The detector elements (pixels) measure 21 μm (cross-track) by 18 μm (along-track). Each camera focal plane contains four separate line arrays, one for each spectral band. The spacing between the line arrays is 160 pm, causing certain bands to "lead" others in spatial position on the ground (see Figure 1); co-registration of the data is accomplished in ground data processing.

The MISR CCD architecture is based on standard 3-phase, 3-poly, n-buried channel silicon detector technology. Thinning of the poly gate over the active pixels increases the detectors' quantum efficiency in the blue spectral region. Full well capacity is 10^6 electrons with read noise < 20 electrons, yielding a large dynamic range for the devices. The signal chains amplify and convert the CCL) video into 14 bit digital numbers. To minimize dark current andradiation sensitivity. the CCD's are operated at -5°C using a single stage Thermo-Electric Cooler (TEC) in each focal plane.

A focal plane filter assembly defining the four optical bandpasses is placed about 1.5 mil

above the CCD. The camera filters are mosaicked arrays of four separate medium band filters. Masks are placed over the epoxy bond lines between the different filters in order to prevent white light from leaking to the focal plane. The filters use ion assisted deposition technology to insure stable and durable coatings which will not shift or degrade with age or environmental stresses.

Electrically, each camera is relatively autonomous with its own power supply and serial data interfaces. The power supplies are 25 kHz sine wave units, providing high efficiency and low noise performance. The camera digital electronics provide interfaces to the system electronics controlling the camera as well as all the drive and timing signals to the CCD focal plane, the double correlated signal chain, and the engineering signal conditioning (ESC) circuits. The signal chains are hybrids, and all camera digital circuits reside on field-programmable gate arrays (FPGA's). These technologies provide for high packing densities.

C. On-Board Calibrator

A key component of the MISR On-Board Calibrator (OBC) is a pair of deployable diffuser panels. These are covered with Spectralon, a pure polytetrafluoroethy lene (Teflon) polymer resin which is compressed and sintered. While not in use the panels are stowed and protected. At approximately monthly intervals the panels will be deployed for calibration. Over the North Pole, the forward-mounted panel will swing aftward to reflect diffused sunlight into the fields-of-view of the aftward-looking and nadir cameras. Over the South Pole, the aftward-mounted panel will swing forward for calibration of the forward-looking and nadir cameras. The nadir camera will provide a link between the two sets of observations.

The diffuse calibration targets are monitored in-flight by radiation-resistant *p,* intrinsic, and *n* doped (PIN) photodiodes and high quantum efficiency (HQE) diodes, These diodes establish the radiornetric scale upon which the instrument calibration is based. The PIN photodiodes are fabricated four to a package, each diode filtered to a different MISR spectral band. Five such packages are used. Two view in the nadir direction, two in the Df and Da camera directions, and one package is mechanized on a goniometric arm to monitor the angular reflectance properties of the panels. The calibration electronics consists of the calibration diode preamplifiers and the ESC circuits associated with the diodes.

The HQE's are in a "trap" configuration, in which three silicon photodiodes arc arranged in a package so that light reflected from one diode is absorbed by another diode. The output of each diode is summed in parallel, resulting in near 100% quantum efficiency. A single spectral filter per package is used, and four such packages provide coverage at the four MISR wavelengths.

The OBC will be used to provide camera response as a function of input radiance, as established by the diode detector standards. Ground data processing of the resulting radiometric transfer curves will be performed on a per-pixel basis to provide the coefficients fot an analytic equation relating camera data number to radiance. This radiance scaling will be applied to MISR data routinely, prior to any further data processing. Further information about the MISR calibration program is contained in *[3]*.

D. System Electronics

All MISR system electronics are redundant, having an A side and a B side, to avoid the possibility of a single-point failure. The system electronics consist of power supplies, logic units which include the firmware to control the instrument prior to loading of the flight software, data management units, and 1750A computers, programmed in Ada, with 1553-type interfaces to the spacecraft. The 1553 interface is used for all commanding, instrument housekeeping data transmittal, flight software loading, and memory readout. The system electronics also provide the high-rate data interface, as well as camera, power, and mechanism controls. System-wide temperature, voltage, and current measurements are provided by a system ESC circuit. All nine of the camera TEC's are powered by the system power supply and placed in series; however, a diode. is placed in parallel with each TEC such that a single failure will not disable the entire string.

As in the cameras, all of the custom digital circuits used in the system electronics reside in FPGA's. These include the logic to enable buffering the CCD data to provide 2 sample x 2 line, 4 sample x 4 line, or l sample x 4 line averages, in addition to the configuration in which pixels are sent with no averaging (1 sample x 1 line). The averaging capability is individually selectable within each of the 36 channels. The system electronics also provide an additional form of data compression by reducing the 14-bit camera outputs to 12 bits through a digital look-up table that square-root encodes the data numbers. Square-root encoding minimizes quantization error at low

signal levels at the expense of increased error at high signal levels, where photon noise dominates. Reversal of the square-root encoding takes place during the early stages of ground data processing.

111. INSTRUMENT OPERATIONS

From the 705-km orbit of the EOS-AM 1 spacecraft, the zonal overlap swath width of the MISR imaging data (that is, the swath seen in common by all nine cameras along a line of constant latitude) is designed to be at least 360 km in order to provide multi-angle coverage of an entire latitude circle in 9 days at the equator, and 2 days near the poles. The cross-track field-of-view and sample spacing of each pixel is 275 m for all of the off-nadir cameras, and 250 m for the nadir camera. Along-track footprints depend on view angle, ranging from 214 m in the nadir to 707 m at the most oblique angle. However, sample spacing in the along-track direction is 275 m in all cameras as a consequence of the 40.8 msec line repeat time of each channel.

There are 14 operational modes of the MISR instrument. Instrument engineering data are always provided over the low-rate 1553 interface. When the instrument is operating under control of the flight software, packetized instrument data, including engineering data, CCD imagery, motor current information, and OBC measurements, are available over the high rate data interface. A brief description of each mode follows.

1) *Off.* This mode is used during launch or at any time the instrument is dormant. All subsystems are unpowered with all mechanisms closed or stowed.

2) Survival. In this mode, the instrument is off with the exception of an A or B string of survival heaters.

3) Start-up. When power is first applied to the instrument, it powers up the computer and system electronics on the selected instrument side (A or B). The power supply for the camera support electronics is powered to a standby level.

4) Safe. This mode is used in response to conditions which have the potential for jeopardizing the mission. Transition to Safe Mode will cause all calibration panels to stow, the goniometer, cameras. and diodes to turn off, and optical bench and instrument replacement heaters to turn on.

5) Safe-Exit. This is a transition mode out of Safe Mode that is activated by commanding either calibration panel or the goniometer to move, or a camera to turn on.

6) *Pre-Memory Load.* The nominal configuration for this mode is for all cameras, TEC'S, optical bench heaters, focal plane heaters, and diodes to be off, in preparation for loading the instrument flight software.

7) Engineering. This mode provides engineering telemetry over the 1553 low-rate data interface as well as packetized engineering data over the high-rate interface. Nominally, all cameras, diodes, and mechanisms are off, and only the system electronics are powered.

8) Global. This mode provides continuous operation of the cameras on the day side of the orbit, Global coverage in each instrument channel is provided by commanding the corresponding signal chain to operate continuously in a selected resolution mode. Standard geophysical data products will be generated using Global Mode data. Current plans are to acquire global data sets by operating the red band of all cameras and all bands of the nadir camera in 1 x l (no averaging); the blue band of the C and D cameras in 1x4; and the remaining channels in 4x4 averaging, as required by the geophysical retrieval algorithms *[4] - [8].*

9) *Local.* This mode provides high resolution (1 xl) images in all four bands of all nine cameras for selected Earth targets. This is accomplished by inhibiting pixel averaging in all bands of each of the cameras in sequence, one at a time, beginning with the first camera to acquire the target (Df) and ending with the last camera to view the target (Da). The instrument geometry limits the downtrack length of Local Mode targets to about 300 km.

10) Calibration North. This mode is used when the spacecraft is in an orbital position at which the deployed forward-mounted calibration panel is illuminated by the Sun. The instrument gathers science data from the An, Aa, Ba, Ca, and Da cameras and all diodes. CCD calibration data wilt be obtained by cycling each channel through the various averaging configurations during the calibration period. This mode will be used on a monthly basis during routine mission operations, although early in the mission it will be used more frequently.

1 1) Calibration South. This mode is used when the spacecraft is in an orbital position at which the

deployed aftward-mounted calibration panel is illuminated by the Sun. The instrument gathers science data from the An, Af, Bf, Cf, and Df cameras and all diodes. In other respects, this mode operates in similar fashion to Calibration North.

/2) *Calibration Diodes.* This mode enables collection of both camera and diode science data on the day side of the orbit. The goniometer-mounted diodes are on but the mechanism is not actuated. The cameras remain in the same averaging configuration used for Global Mode.

13) Calibration Dark This mode enables collection of both camera and diode science data on the dark side of the orbit. The goniometer motor is actuated for a portion of the sequence. Each CCD channel is cycled through all of the averaging configurations in order to provide an assessment of dark current and the influence of goniometer actuator activity on instrument noise.

14) Test. In this mode the instrument outputs a fixed pattern to the high rate data interface and shuts off engineering data flow to this interface.

IV. GEORECTIFICATION AND REGISTRATION

Spatial co-registration of the 36 channels of data from the instrument is an essential requirement of all of the MISR geophysical retrievals. This is accomplished during ground data processing. Instrument-related geometric distortions will be accounted for by extensive geometric camera calibration. The results of pre-flight and in-flight geometric calibration will be used to construct a camera model, which utilizes the rigid relation between the cameras to describe the instrument pointing in terms of static and dynamic (temperature dependent) parameters.

A. Use of Space-Oblique Mercator Map Grid

A common map projection, or grid, for the georectified radiances is established to provide the required co-registration. Space-Oblique Mercator (SOM) is used for this grid because its projection meridian nominally follows the spacecraft ground track and a constant distance scale is preserved along that track, thus minimizing distortion and resampling effects. The map resolution of the projection will also be matched to the horizontal sampling mode of each camera channel. The horizontal datum for each projection is the World Geodetic System 1984 (WGS84) ellipsoid. A

separate projection will be established for each of the paths of the 233 repeat orbits of the EOS 16-day cycle. The SOM-gridded images and geophysical data constitute an intermediate step to the Earth-based map projections to be used for global mapping at higher processing levels. Two types of SOM projection will be used for MISR data *[9]*.

1) Terrain Projection. Certain retrieval algorithms require the radiances from all nine cameras of MISR to be co-registered and projected to the surface terrain. This is achieved by projecting the images to a surface defined by a digital elevation model (DEM) in order to account for angle-dependent topographically induced misregistrations. In areas where it is necessary to correct for topography, the position and pointing information contained in the spacecraft ancillary data may not provide sufficiently accurate ground location. The MISR terrain projection algorithm will therefore utilize matching to a set of reference images to supplement the spacecraft navigation data. The reference orbit imagery is to be constructed from relatively cloud-free MISR data collected early in the EOS-AM1 mission.

2) Ellipsoid Projection. Other retrieval algorithms require the radiances from all nine cameras of MISR to be projected to a surface defined by the WGS84 ellipsoid. For example, this surface is where camera-to-camera stereo matching will be performed to determine cloud-top altitude. Projection of the imagery from the nine cameras (and individual bands) to a smooth ellipsoid is not as sensitive to viewing geometry as the terrain-projection algorithm. Therefore the spacecraft attitude and position are used as reported (but improved by the calibrated camera model and static corrections obtained from matching) to determine an intersection with the surface ellipsoid, Then, resampling of the imagery to the SOM projection is performed.

V. CLOUD STUDIES

A. Background

As a result of their large areal extent, high albedo, and variability on many length and time scales, clouds play a major role in governing the Earth's energy balance. Models of [he response of the Earth's climate system to, tor example, the increase in trace gases, are severely limited by our present ignorance of the feedback processes associated with changes in cloud amount and cloud properties. Deriving from its ability to measure any scene from multiple directions. MISR

will improve our ability to model cloud-radiation interaction by taking into account the variable structure of broken cloud fields, and will obtain hemispherical fluxes with resolution sufficient to discriminate between cloud-filled and cloud-free scenes. The overall scientific objectives of the MISR cloud retrievals are described next.

/) Cloud Detection and Screening. Cloud detection is used to (a) determine whether a scene is classified as clear or cloudy for the purpose of choosing the angular integration coefficients which are used in estimating top-of-atmosphere (TOA) albedos, (b) calculate regional cloud cover, and (c) determine whether a scene is clear enough to perform aerosol and surface. retrievals. Applying traditional cloud screening methods to each MISR camera is a challenging problem given the small number of spectral channels available, none of which are longward of 1 μm. As a result, only a few simple cloud detection observable are constructed from arithmetic operations on the camera radiances. However, MISR affords the opportunity to apply multi-angle methods as well, including stereophotogrammetric techniques and angular signature-based approaches.

2) Cloud Classification. Cloud classification by MISR will partition clouds into categories distinguished by parameters such as cloud-top elevation and texture or degree-of-brokenness (e.g., strati form vs. cumuliform). Reliable estimates of cloud-top altitude are required to model the three-dimensional field of radiative fluxes which play a critical role in climate feedback. Cloud-top elevation is conventionally retrieved using thermal-infrared brightness temperatures together with temperature-pressure profiles from objective analyses of meteorological data. Stereoscopic observations from satellite provide an independent, and wholly geometric means to obtain this information without assumptions about the relationship between cloud-top radiative temperature and cloud-top pressure [/0] - [12]. Recent experience with automated stereo matching algorithms as applied to AVHRR [/3], SPOT [/4] and Along-Track Scanning Radiometer (ATSR) *[15]* suggest that the fore-aft viewing strategy of MISR is a viable means for retrieving cloud height. Once the cloud images are co-registered to the appropriate altitude level. multi-angle textural parameters will also be calculated.

3) Characterization of Cloud Climatic Effects. Many theoretical studies have established that plane-parallel representations of cloud fields introduce large errors in the parameterization of radiation for climate models *[16],[17].* Cloud modeling must consider not only the effects of

individual cloud shape but also interactions such as shadowing and multiple scattering between clouds. Diffusion of radiation through the cloud sides and side illumination causes the angular reflectance of cumuli form cloud fields to differ markedly from those of strati form fields *[18],[19]*; therefore, careful scene classification and angular integration schema will be implemented by MISR to obtain accurate estimates of TOA albedo.

B. Retrieval Strategy

Cloud screening involves discriminating between clear and cloudy pixels in an image. Radiance threshold techniques work on a pixel-by-pixel basis, and single or multiple-channel thresholds are defined which are then used to divide clear and cloudy pixels. The. observable that are used for MISR data depend on whether the observations are made over water or land. Each observable will be tested by comparing to thresholds derived from time cumulated statistics over a particular geographical region. The thresholds are a function of view angle, sun angle, relative view-sun azimuth angle, time, and surface type. The result of this process, applied to each camera, is known as the Radiometric Camera-by-camera Cloud Mask (RCCM).

Stereoscopic detection of clouds (and, if present, volcanic plumes) is based on height retrieval that uses the contrast measured by different cameras, and a combination of feature-based and area-based matching techniques [20]. Determining the heights from multi-angle views involves detecting disparities (i.e., horizontal spatial offsets in the imagery resulting from the parallax obtained by viewing at different angles). An accurate stereo matching algorithm is used to retrieve velocity and height values for a sparse subset of features in the MISR imagery. By selecting triplets of cameras with non-symmetric and oblique view zenith angles, we are able to separate the heights and velocities in the data reduction. Once the motion field has been derived, the conjugate points of stereo matchers applied to high resolution data from pairs of cameras are used to retrieve a height field. The results are used to establish a Stereoscopically -Derived Cloud Mask (SDCM).

Detection of high cirrus is also important to MISR. Nadir imagers cannot always detect cirrus clouds due to restricted phase angle coverage. Therefore, the multi-angle strategy will be used in a novel way. Di Girolamo and Davies [21] have developed a method known as Band-Differenced Angular Signature (BDAS), which takes advantage of the difference in the Rayleigh signal above

high clouds between blue and red or near-IR wavelengths as a function of angle. High clouds have a unique signature that distinguishes them from clear sky and low-level clouds. Application of this technique generates an additional classifier, known as the Angular Signature Cloud Mask (AS-CM).

In order to establish a parameter that serves the purpose of providing a classification scheme that incorporates cloud altitudes, and which also serves as a dynamic (i.e., spatially varying) reference altitude for co-registering the multi-angle views, a reference level known as the Reflecting Level Reference Altitude is established. The RLRA is derived from the stereoscopic height field. Physically, it corresponds to the main reflecting layer, and depending on atmospheric conditions will typically be either the tops of bright clouds or the surface. The RLRA is defined over subregions measuring 2.2 km x 2.2 km. For scene classification purposes, the stereoscopic heights used in deriving the RLRA are also used to generate regional altitude-binned cloud fraction metrics. The RLRA is also used as a common reference altitude for projecting the multi-angle bidirectional reflectance factors, from which albedos and textural parameters will be derived.

The calculation of directional hemispherical reflectance (DHR), or albedo, involves an angular integration of bidirectional reflectance factors (BRF's) over the upwelling hemisphere. MISR's arrangement of nine cameras provides good coverage in zenith angle; however, the fore-aft views provide sampling at only two azimuth angles for each zenith angle. (Denser coverage in azimuth angle would require binning data acquired on different orbits, and thus would not represent an instantaneous view of the same scene). Supplemental information to mode] the azimuthal dependence of BRF is therefore required to obtain the most accurate estimates of albedo. This is accomplished by choosing an Azimuthal Model (AZM) to facilitate the angular integrations. Selection of the appropriate AZM coefficients depends on solar zenith angle, whether a scene has been classified as clear or cloudy by the cloud detection process, and if cloudy, on an estimate of the cloud phase (liquid or ice), cloud texture, brightness, and altitude (to account for Rayleigh scattering) *[22]*.

The probability of scene heterogeneity increases rapidly with scene size, making the relationship between area-averaged radiance and area-averaged scene properties (e. g., cloud liquid water) progressively more biased *[23]*. By matching albedos to scene characteristics, especially cloud in-

formation, local albedos can be corrected for azimuthal bias more effectively than albedos of larger areas. The local al bedos can then be summed over larger areas to produce al bedos of more heterogeneous scenes at coarser resolution. Two coarse resolution albedos, defined over regions measuring 35.2 km x 35.2 km and referenced to 30-km altitude, are defined for MISR. We define the "restrictive" albedo to be the one obtained using angular integration of the observed BRF's over the given region only, and the "expansive" albedo to be the one obtained using integration over all relevant surrounding regions, that is, all regions influencing the radiative flux leaving the top of the atmosphere in an area extending to a few hundred kilometers on each side. As a result, the restrictive albedo is the more useful measure of scene-dependent properties such as column absorption, and is analogous to earlier single view determinations of the TOA albedo (e.g., the Earth Radiation Budget Experiment, ERBE), whereas the expansive albedo corresponds to what would be measured by an albedometer at 30 km altitude.

VI. AEROSOL STUDIES

A. ***Background***

Aerosols are solid or liquid airborne particulate of various compositions, frequently found in stratified layers. Generally, they are defined as atmospheric particles with sizes between about 0.1 μm and 10 μm, though the sizes of condensation nuclei are typically about 0.01 μm. Under normal conditions, most of the atmospheric aerosol resides in the troposphere. Natural sources (e.g., dust storms, desert and soil erosion, biogenic emissions, forest and grassland fires, and sea spray) account for about 90% of this aerosol, with the rest resulting from anthropogenic activity *[24]*. The background tropospheric aerosol is temporally and spatially variable. The overall objectives of the MISR aerosol retrievals are described next.

1) Characterization of Aerosol Climatic Effects. Aerosols are thought to play a direct role in the radiation budget of Earth, on regional and hemispheric length scales *[29]*,*[30]*; however, their net radiative effect, i.e., whether they heat or cool the surface, depends on their optical properties and the albedo of the underlying surface. It is believed that on the global average, aerosols provide a net cooling effect. Northern hemispheric sources are thought to be sufficiently large so that the net radiative effect of anthropogenic sulfate aerosols alone is comparable in size (of order 1-2 W/m^2), though opposite in sign, to the anthropogenic CO_2 radiative forcing *[31]*. Aerosols may also play

an indirect role in the Earth's radiation balance, through their effects on clouds *[32]*, with a radiative effect of similar magnitude. MISR global aerosol retrievals will be used to obtain aerosol optical depth and place constraints on aerosol particle types.

2) Mapping of Aerosol Distribution. The lifetimes of tropospheric aerosol particles are thought to range from about a week to a little over a month. These include sulfuric acid particles, which form photochemically from SO_2 *[25]*. Because these lifetimes are short relative to global atmospheric mixing times, spatial-temporal patterns are often indicative of sources and sinks. For example, particles off the northwest coast of Africa and the east coast of central Asia are generally interpreted as being desert dust, those around Latin America in northern spring as forest fire particles, and those off the east coasts of Japan and North America as industrial particles [26]. However, current satellite retrievals from the Advanced Very High Resolution Radiometer (AVHRR) *[27]* are otherwise unable to distinguish different particle types or compositions, since they are based on measurements at a single wavelength and angle of view. Their algorithm to convert observed radiance to aerosol optical depth assumes particles of a fixed composition and size. Total Ozone Mapping Spectrometer (TOMS) ultraviolet satellite data detect aerosol presence but the conversion to quantitative optical properties is sensitive to assumptions about aerosol altitude and aerosols in the boundary layer (the lowest 1 km of the atmosphere) are not observable *[28]*. MISR's extensive coverage in both wavelength and view angle provides the means to distinguish different particle types based on their physical and optical properties. This will improve our ability to constrain the underlying sources, and to varying degrees, sinks and lifetimes, that govern their concentration in the troposphere.

3) Atmospheric Corrections. The goal of any atmospheric correction scheme is the accurate retrieval of surface reflectance or surface-leaving radiance from TOA radiances. It is well established that scattering and absorption by aerosols are responsible for dramatic modifications of the spectral content of remotely sensed images of the Earth's surface, leading to classification errors *[33]*, reduced accuracy of image products such as vegetation maps *[34]*, and a degradation in the accuracy of quantitative estimates of surface radiative properties. The retrieval of aerosol scattering properties by the MISR algorithm is an essential precursor to retrieval of surface properties using MISR data.

B. Retrieval Strategy

In order to constrain the MISR aerosol retrievals, it is advantageous to make reasonable use of what is known about the types of aerosols that are found in the troposphere. In general, tropospheric aerosols fall into a small number of compositional categories, which include sea spray, sulfate/nitrate, mineral dust, biogenic particles, and urban soot. Approximate size ranges, and the proclivity of each particle type to adsorb water under increasing relative humidity are also known. Therefore, the MISR team has chosen an approach in which the physical and chemical (and therefore optical) properties of candidate aerosols are completely prescribed. The advantages of this approach, in contrast to a purely "generic" representation in terms of effective single scattering albedo, effective size distribution, and effective phase function, are that it potentially enables identification of aerosol sources and provides the means of extending aerosol properties retrieved at the MISR wavelengths to other spectral regions, which will be useful for comparisons with other sensors and for model validation. To this end, a review of published aerosol climatologies was performed (including *[35] - [38]* and many others). Aerosol attributes typical of natural conditions as described in these references (such as compositional and size classes) are adopted in the MISR retrievals. Based on these assumptions, the aerosol amount and specific spatial and temporal distributions are retrieved from the MISR observations.

The MISR aerosol retrieval strategy works as follows: Based on the physical and compositional properties of known types of aerosols, forward radiative transfer calculations are performed to provide various components of the atmospheric radiation field in the 36 MISR channels. These are stored in a pre-established look-up table, and top-of-atmosphere radiative properties of mixtures of these "pure" aerosols is accomplished during the retrievals using a modified linear mixing theory *[39]*. The results will be compared with the MISR observations to determine those models that provide good fits to the data, and to retrieve aerosol optical depth. Three retrieval pathways, one over water and two over land, are utilized. For each of these retrieval paths, optical depth constraints. such as the maximum allowable optical depth, based on the darkest radiance observed in the scene, are calculated.

Because of the reflectance uniformity of large water bodies (e.g., the ocean), and the fact that deep water bodies have negligible water-leaving radiance at red and near-infrared wavelengths,

considerable progress has been made in development of algorithms to retrieve aerosol properties over dark water. Under the assumption of an aerosol model (i.e., specification of particle size distribution, particle shape, and complex refractive index), it is possible to relate observed radiance to aerosol optical depth. Such modeling has been applied to the retrieval of aerosol concentration from Landsat *[40]*, /41] and AVHRR *[27]*, *[42]* - *[44]*. However, these techniques can incur systematic biases due to the inherent assumptions, such as spherical particles of "sulfate" composition, a specific Junge distribution of sizes, and a lambertian surface of reflectivity 0.015 *[45]*.

Substantial improvements in the retrieval of aerosol over ocean and other dark water bodies are possible with MISR. Multi-angle radiances, which are governed strongly by the shape of the aerosol scattering phase functions, provide additional information with which to refine the aerosol model used in the retrieval of optical depth. For example, Kahn et al. *[46]* have shown that MISR data will be capable of distinguishing spherical from non-spherical particles, and additional sensitivity studies demonstrate the ability of multi-angle data to distinguish among particles with small, medium, and large modal sizes and to provide an estimate of particle absorption *[47]*.

The retrieval of aerosol optical depth over land is less well developed than the dark water case because of the higher brightness and heterogeneity of the land surface. As a consequence, separation of the land-leaving and atmosphere-leaving signals in remotely sensed radiances must be performed in order to retrieve aerosol properties from the measured signal. The simplest means of determining the atmospheric contribution to the satellite signal is to make an assumption about the surface reflectivity or albedo. Locations where the surface boundary condition is believed to be reasonably well understood are areas covered by Dense Dark Vegetation (DDV). A method based on imaging over DDV has been investigated *[48]* and forms the basis of the aerosol retrieval over land *[49]* to be used at single angles of view by the Moderate-resolution Imaging Spectroradiometer (MODIS), also on the EOS-AM l platform. MISR extends this approach by assuming a parametric model for the shape of the angular reflectance distribution in the blue and red spectral bands *[50]*. The functional form is a modification of the Rahman-Pinty-Verstraete model *[51]* and the absolute reflectance in the two spectral bands, along with aerosol optical depth, are treated as free parameters to be determined during the retrieval process.

Since dense vegetation is found only over a portion of the land surface, other methods are

required to extend the aerosol retrieval spatial coverage. Separability of the surface-leaving and atmosphere-leaving signals over terrain with heterogeneous surface reflectance provides the foundation of the third aerosol retrieval pathway. The heterogeneous land algorithm differs from the dark water and DDV retrieval methods in that it does not use the observed radiances directly, but instead uses the presence of spatial contrasts to derive an Empirical Orthogonal Function (EOF) representation of the angular variation of the scene reflectance, which is then used to estimate the scene path radiance (the radiance field reflected from the atmosphere without interacting with the surface) *[52]*. This is used in turn to determine the best-fitting aerosol models and associated optical depth by comparing the results with the pre-computed values contained in the look-up table. Sensitivity studies on both the DDV and EOF methods imply that MISR data will afford unique approaches to retrieving aerosol properties over the land surface.

VII. SURFACE STUDIES

A. Background

Land surface processes are important components of the terrestrial climate system *[53]*. In particular, continents affect the climate system because of (a) their roughness on many length scales, which affects the dissipation of atmospheric kinetic energy through friction and turbulence and modifies the planetary atmospheric flow, (b) their relatively small heat capacity, compared with that of the oceans, which induces a range of dynamic perturbations, from sea-breezes to monsoons, (c) their albedo and, to a lesser extent, emissivity, which are highly variable in space and time, and which control the absorption of solar and the emission of thermal radiation, respectively, hence the bulk of the energy available in the climate system, and (d) their hosting of most of the biosphere (over 99% by mass), which exerts significant controls on the exchange of heat, moisture, and chemical compounds within the climate system. Over oceans, roughly the same amount of photosynthesis as is performed by land vegetation occurs as a result of marine phytoplankton, which are the basic link in the ocean food chain. The overall scientific objectives of the MISR surface retrievals are described next.

/) Surface Radiative Fluxes. The bulk of the solar energy provided to the troposphere is absorbed at the lower boundary (oceans and continents) and then re-emitted to the atmosphere through the fluxes of sensible and latent heat, as well as in the form of thermal radiation. Accurate descriptions

of the interactions between the surface and the atmosphere require reliable quantitative information on the fluxes of energy (all forms), mass (including water and $C0_2$), and momentum, especially over terrestrial areas, where they are closely associated with the rates of evapotranspiration and photosynthesis. Many of these processes and interactions directly affect the reflectance of the surface *[54]* - [56]. Reflectance measurements, which can be acquired by remote sensing, are therefore particularly useful to describe and predict these surface-atmosphere interactions. Clearly, the usefulness of such measurements is not limited to vegetated areas, as all significant modifications of surface properties, whether due to natural or human-induced causes, tend to affect this property. It is well known that natural surfaces do not behave as lambertian scatterers but exhibit anisotropic reflectance properties which depend on the characteristics of the surface. Integration of the retrieved directional reflectance over the whole hemisphere of viewing angles defines the hemispherical reflectance (spectral albedo) of the surface.

2) Land Surface Classification. The evolution of terrestrial ecosystems is difficult to monitor at the surface, and satellite platforms provide a unique opportunity to carry out extensive surveys with comprehensive spatial coverage and high time resolution. Detection of ecophysiological change on the land surface, resulting from natural processes (canopy succession and species replacement) or anthropogenic activities (e. g., deforestation, acid rain), necessitates accurate, repeatable measurements of the surface that can be used for landscape classification. Hall et al. *[57]* showed how time series of satellite data could be used to monitor ecosystem dynamics over large areas, a task that was not feasible prior to the advent of satellite remote sensing. Although spectral data provide some information on the physiological state of vegetation, inference of the structural properties of the three-dimensional vegetation stand is also required, and it is difficult to determine canopy architecture and states (e. g., biomass, leaf area index) from a single view angle *[58], [59].* Multi-angle information enables the use of physically-based models to infer canopy structure *[60].*

3) Biological Productivity. The productivity of land vegetation is related, among other factors, to the amount of incident photosynthetically active radiation (400 - 700 nm) absorbed by the photosynthesizing tissue in a canopy, parametrized by the ratio of absorbed to incident radiation, FPAR. An accurate specification of FPAR is a crucial factor in the estimation of large-scale productivity and carbon budget models *[61] - [63].* Over oceans, the concentration of chlorophyll

a and its degradation products (known as phaeopigments) provide an estimate of the rate of biological productivity in the marine environment. The primary instrument for assessing ocean productivity on EOS-AM I is MODIS. When the satellite passes over the solar equator, some imagery is lost due to sun glint. Because MISR acquires images continuously at several angles, has good signal-to-noise ratio at low signal levels, and provides high accuracy aerosol retrievals, ocean color data uncontaminated by sun glitter will be obtained in this region.

B. Retrieval Strategy

Before surface retrievals can be performed within a given region, atmospheric parameters need to be determined by means of an aerosol retrieval. Then, over land, the following sequence of surface retrieval activity is performed on all suitable 1.1 km samples within a region [64]. First, the hemispherical-directional reflectance factors (HDRF's) for all available camera views and the bihemispherical reflectance (BHR's) are determined for the four MISR spectral channels. The HDRF's and BHR's are surface reflectance properties for illumination conditions of the ambient atmosphere (i.e., direct and diffuse sunlight) and are retrieved with a minimum number of assumptions. The HDRF, because it is defined for the actual illumination conditions, is useful for climate modeling and for comparison with field measurements. Using the HDRF's as a starting point, the corresponding bidirectional reflectance factors (BRF's) and the directional-hemispherical reflectances (DHR's) are determined. These quantities are defined for illumination by direct sunlight only, and thus are more useful for the purpose of determining the physical state of the surface from angular shape information. Their retrieval requires assumption of a model describing the bidirectional reflectance properties of the surface, because it is necessary to correct for the diffuse skylight illumination. We use a modified form of an empirically-derived, parametric formulation to carry this out *[51]*.

From the spectral BHR's and DHR's the PAR-integrated BHR and DHR are obtained. The PAR (photosynthetically active radiation) band covers the 400-700 nm wavelength range, allowing three of the four MISR channels to be used in the integration. The PAR-integrated BHR and DHR are a measure of the amount of PAR absorbed by the surface (vegetative and non-vegetative) under ambient and direct illumination conditions. Then, a Normalized Difference Vegetation Index (NDVI) derived from red and near-infrared DHR's will be used to distinguish vegetated from non-

vegetated terrain. These NDVI values do not depend on view angle and have been corrected for atmospheric effects. Over vegetated land, the green leaf-area index (LAI) is estimated from a comparison of the retrieved spectral BHR's and DHR's with a look-up table containing results of detailed radiative transfer modeling of the plant canopy biome types. Six biome types are considered: grasses and cereal crops, shrublands, broadleaf crops, savanna, broadleaf forests, and needle forests. All canopy models which pass this comparison test are then put through another discriminator by comparing their directional reflectance to the retrieved BRF's. This process provides a land surface classifier along with an associated LA]. FPAR, the fractional amount of incident PAR absorbed by vegetation canopies only (and not the understory) is then estimated.

Correction for atmospheric scattering over oceans is essential for studies of ocean color because the low reflectance of the ocean surface (away from sun glitter) results in the signal being dominated by Rayleigh and aerosol backscatter. Gordon et al. [65] have developed operational atmospheric correction algorithms for use with Coastal Zone Color Scanner (CZCS) imagery. The multi-angle coverage of MISR enables further refinement of the aerosol model and the application of rigorous surface retrieval algorithms *[64]*. The ocean surface retrieval process is performed only for the tropical ocean, which for our purpose is limited to a 600 km wide band centered on the geographic equator. Phytoplankton pigment concentration is estimated at a spatial resolution of 1.1 km, using the retrieved water-leaving radiances in the MISR blue and green bands as inputs to the CZCS bio-optical pigment algorithm. With the MISR spectral band set, chlorophyll pigment concentration is estimated by forming the ratio of the equivalent reflectance in the blue (446 nm) and green (558 nm) bands. Since MISR does not include bands between 446 nm and 558 nm, only the low phytoplankton pigment concentration range (O -1 mg pigment/m^3) will be available; however, this should be sufficient for most of the tropical oceans.

VIII. GROUND DATA SYSTEM

A. MISR Science Data Processing

The MISR Science Computing Facility (SCF) at JPL and Distributed Active Archive Center (DAAC) at NASA Langley represent the primary entities in which the functions of MISR science data processing will be implemented. The DAAC, which is shared with several other EOS instruments, is the facility at which software incorporating MISR science algorithms will operate in a

high volume, real-time mode to produce standard science data products. The generation of science data products can be divided into six subsystems within the product generation system. Each subsystem has at least one primary output product, but may have other secondary output products. It is convenient to conceptualize the processes within these subsystems as occurring in sequence, with the predecessor producing at least one complete product, a portion of which is the primary input for the successor. Each of these subsystems correspond to a processing level of a product generation flow, as shown in Figure 4. These levels conform generally to the EOS scheme from Level 1 to Level 4.

Standard products cannot be generated at the DAAC independently of the rest of the MISR science data system. They are critically dependent on calibration parameters and other look-up data, such as threshold datasets, atmospheric climatologies, aerosol and surface model datasets and the like, which are produced at the SCF. Updates to these data structures occur infrequently compared to the rate of standard product generation, and therefore fit into the more limited processing capabilities of the SCF. Other essential functions that have activities at the SCF include quality assessment, algorithm and data product validation, software development, and instrument operations.

IX. CONCLUSIONS

Some of the ways in which the multi-angle viewing strategy of MISR provides unique information about clouds, aerosols, and surfaces are summarized below.

1) Three-dimensional structure characterization. The angular scattering "signature" of complex scenes such as cloud fields and vegetation canopies is expected to be diagnostic of their three-dimensional geometry. The high resolution of the MISR data (275 m - 1.1 km) facilitates the classification of unique scene types.

2) Stereoscopic height and wind retrieval. The nadir and several of the off-nadir cameras will be used stereo-photogrammetrically to estimate cloud-top or plume-top altitudes, for the purposes of regional scene classification and for co-registering the multi-angle views to a common reference level. Unlike single camera-pair stereo, multi-camera disparity measurements obtained at both small and large base-to-height ratios from satellite altitudes enable compensation for the effects of

motion due to wind.

3) Aerosol composition identification. The nine cameras provide coverage in scattering angle, which is the angle between the direction of the Sun's rays and the direction to the sensor. The phase function, which is dependent on scattering angle, differs among aerosols of varying compositions and sizes.

4) Aerosol optical depth retrieval. The compositional information provided by the scattering phase functions, coupled with the fact that the oblique MISR viewing angles accentuate the aerosol signal because of the increased optical path length through the atmosphere, enable new methodologies for retrieving aerosol optical depth over land and ocean.

.5) *Cirrus detection and characterization.* The oblique viewing angles of the cameras at high off-nadir angles, particularly the C and D cameras, accentuate the signal of high thin clouds (cirrus) because of the increased optical path length through the atmosphere. This forms the basis for a novel technique to detect cirrus. The single-scattering phase function of cirrus is not well known, and MISR data will provide new information on cirrus reflective properties.

6) *Scene-dependent albedo determination.* The high spatial resolution, multi-angle observations provide a novel methodology for determining the hemispherical albedo at the top-of-atmosphere and surface.

7) *Surface classification.* NDVI retrieved from MISR data is independent of view angle and atmospheric conditions and will be used to distinguish vegetated from non-vegetated land. Spectral hemispherical reflectance and bidirectional reflectance factors will be used to establish the land biome type. Accurate multi-angle aerosol and surface retrievals over ocean will provide assessments of biological productivity in tropical marine environments.

For further information about the MISR experiment, the reader is invited to peruse our World W ide Web site at *http://www-misr.jpl.nasa.gov*.

X. ACKNOWLEDGMENTS

The authors gratefully acknowledge the efforts of the MISR hardware and software engineering teams, and a host of graduate students, post-doctoral researchers, and research assistants who have made substantial contributions to the experiment, In particular, we thank Nadine Chrien, Gary Francis, Barbara Gaitley, and Stuart McMuldroch for the analyses leading to the performance values included in Tables I - III. We also thank Barbara Gaitley for the photograph in Figure 3. This research is being carried out, in part, by the Jet Propulsion Laboratory, California Institute of Technology, under contract with the National Aeronautics and Space Administration.

XI. REFERENCES

[1] D.J. Diner, C.J. Bruegge, J.V. Martonchik, G.W. Bothwell, E.D. Danielson, V.G. Ford, L.E. Hovland, K.L. Jones, M.L. White, "A Multi-angle Imaging SpectroRadiometer for terrestrial remote sensing from the Earth Observing System," *Internatl. J. Imaging Sys. and Tech. 3, 92-107,* 1991.

[2] C.J. Bruegge, V.G. Duval, N.L. Chrien, B.J. Gaitley, R.P. Korechoff, and E. Hochberg, "MISR prelaunch instrument calibration and characterization results," *IEEE Trans. Geosci. Remote Sens.*, this issue, 1997.

[3] C.J. Bruegge, D.J. Diner, and V.G. Duval, "The MISR calibration program," *J. Atmos. Ocean. Technol. 13,286-299,* 1996.

[4] D.J. Diner, L. Di Girolamo, and E. Clothiaux, "MISR Level 1 Cloud Detection Algorithm Theoretical Basis," *JPL document D-13397, Rev. A,* Jet Propulsion Laboratory, 1997.

[5] D.J. Diner, R. Davies, L. DiGirolamo, A. Horvath, C. Moroney, J-P. Muller, S. R. Paradise, D. Wenkert, and J. Zong, "MISR Level 2 Cloud Detection and Classification Algorithm Theoretical Basis," *JPL document D- 11399, Rev. C,* Jet Propulsion Laboratory, 1997.

[6] D.J. Diner, R. Davies, T. Várnai, C. Moroney, C. Borel, and S.A.W. Gerstl, "MISR Level 2 Top-of-Atmosphere Albedo Algorithm Theoretical Basis," *JPL document D-13401, Rev. C,* Jet Propulsion Laboratory, 1997.

[7] D.J. Diner, W.A. Abdou, T.P. Ackerman, K. Crean, H.R. Gordon, R.A. Kahn, J.V. Martonchik, S. McMuldroch, S.R. Paradise, B. Pinty, M.M. Verstraete, M. Wang, and R.A. West, "MISR Level 2 Aerosol Retrieval Algorithm Theoretical Basis," *JPL document D-11400, Rev. C,* Jet Propulsion Laboratory, 1997.

[8] D.J. Diner, J.V. Martonchik, C. Borel, S.A.W. Gerstl, H.R. Gordon, Y. Knjazikhin, R. Myneni, B. Pinty, and M.M. Verstraete, "MISR Level 2 Surface Retrieval Algorithm Theoretical Basis," *JPL document D-1/401, Rev. C*, Jet Propulsion Laboratory, 1997.

[9] V.M. Jovanovic, M. M. Smyth, J. Zong, and R. R. Ando, "MISR photogrammetric data reduction for geophysical retrievals," *IEEE Trans. Geosci. Remote Sens.,* this issue, 1997.

[10] A.F. Hasler, "Stereographic observations from geosynchronous satellites: An important new tool for the atmospheric sciences," *Bull. Amer. Met. Sot. 62, 194-212, 1981.*

[11] A.F. Hasler, R. Mack, and A. Negri, "Stereoscopic observations from meteorological satellites," *Adv. Space Res. 2, 105-113, 1983.*

/12] D. Lorenz, "Stereoscopic imaging from polar orbit and synthetic stereo imaging," *Adv. Space Res. 2,* 133-142, 1983.

[13] J-P. Muller, "Real-time stereo matching and its role in future mapping systems," Survey & Mapping 89, University of Warwick, 17-21 April 1989, 15 pp., 1989.

[14] T. Day and J-P. Muller, "Digital elevation model production by stereo-matching SPOT image-pairs: A comparison of algorithms," *Image and Vision Computing 7,95-101,* 1989.

[15] J-P. Muller and A. Mandanayake, "Comparison of stereo-derived cloud-top heights with brightness temperature-derived cloud-top pressure," *J. Geophys. Res.*, in preparation, 1997.

[/6] R. Harshvardhan, R. Davies, D.A. Randall and T. G. Corsetti, "A fast radiation parameterization for atmospheric circulation models, " *J. Geophys. Res.* 92, 1009-1016, 1987.

[17] R. M. Welch and B. A. Wielicki, "Stratocumulus cloud field reflected fluxes: The effect of cloud shape," *J. Atmos. Sci.* **41, 3085-3103, 1984.**

[18] J. A. Coakley and R. Davies, "The effect of cloud sides on reflected solar radiation as deduced from satellite observations," *J. Atmos. Sci.* 43, 1025-1035, 1986.

[19] R. Davies, "Reflected solar radiances from broken cloud scenes and the interpretation of scanner measurements," *J. Geophys. Res.* 89, 1259-1266, 1984.

[20] R. Davies, L. Di Girolamo, T. Várnai, A. Horvath, C. Moroney, J-P. Muller, and A. Mandanayake, "Cloud classification using multi-angle satellite measurements: Methodology and simulation," *IEEE Trans. Geosci. Rem. Sens.*, this issue, 1997.

[21] L. Di Girolamo and R. Davies," A Band-Differenced Angular Signature technique for cirrus cloud detection," *IEEE Trans. Geosci. Rem. Sens. 32, 890-896,* 1994.

[22] R. Davies, T. Várnai, C. Bore], and S. Gerstl, "Albedo determination using multi-angle satellite measurements: Methodology and simulation," *IEEE Trans. Geosci. Rem. Sens.*, this issue, 1997.

[23] L. Oreopoulos and R. Davies, "Plane parallel albedo biases from satellite observations. Part I: Dependence on resolution and other factors," *J. Climate*, in press, 1997.

[24] S. J. Williamson, "Fundamentals of Air Pollution," Addison-Wesley, MA, 1972.

[25] R. P. Turco, R.C. Whitten, and O. B. Toon, "Stratospheric aerosols: Observation and theory," *Rev. Geophys. Space Phys. 20, 233-279, 1982.*

[26] R. B. Husar, J. Prospero, and L.L. Stowe, "Characterization of tropospheric aerosols over oceans with the NOAA AVHRR optical thickness operational product," *J. Geophys. Res.* **102, 16889-16909, 1997.**

[27] C. R. N. Rae, L. L. Stowe, and E. P. McClain, "Remote sensing of aerosols over the oceans using AVHRR data: Theory, practice and applications," *Int. J. Remote Sensing* **10,** 743-749. 1989.

[28] J. R. Herman, P. K. Bhartia, O. Torres, C. Hsu, C. Seftor, and E. Celarier, "Global distribution of UV-absorbing aerosols from Nimbus 7/TOMS data," *J. Geophys. Res.* 102, 1691 1-

16922, 1997.

[29] R. J. Charlson, S. Schwartz, J. Hales, R. Cess, J. Coakley, Jr., J. Hansen, J., and D. Hofmann, "Climate forcing by anthropogenic aerosols," Science 255, 423-430, 1992.

[30] J. T. Kiehl and B.P. Briegleb, "The relative roles of sulfate aerosols and greenhouse gases in climate forcing," Science 260,311-314, 1993.

[31] R. J. Charlson, J. Langner, H. Rodhe, C. B. Leovy, and S. G. Warren, "Perturbation of the northern hemispheric radiative balance by backscattering from anthropogenic sulfate aerosols," *Tellus* 43AB, 152-163, 1991.

[32] G. Vali, cd., "Report of the Experts Meeting on Interaction Between Aerosols and Clouds," WCRP-59, WMO / TD-No. 423, 1991.

[33] R. S. Fraser and Y. J. Kaufman, "The relative importance of aerosol scattering and absorption in remote sensing," *IEEE Trans. Geosci. and Rem. Sens. GE-23, 625-633,* 1985.

[34] B. N. Holben, D. Kimes and R. S. Fraser, "Directional reflectance response in AVHRR red and near-IR bands for three cover types and varying atmospheric conditions," *Rem. Sens. Environ.* **19, 213-236, 1986.**

[35] G. A. d'Almeida, P. Koepke, and E. P. Shettle, "Atmospheric Aerosols: Global climatology and radiative characteristics," Deepak Publishing, 1991.

[36] G. M. Krekov, "Models of atmospheric aerosols," in *Aerosol Effects on Climate, S. G.* Jennings, cd., University of Arizona Press, pp. 304, 1993.

[37] E. P. Shettle and R.W. Fenn, "Models for the aerosols of the lower atmosphere and the effects of humidity variations on their optical properties," Air Force Geophysics Laboratory, Hanscomb AFB, MA 01731, AFGL-TR-79-02 14, 1979.

[38] World Climate Programme WCP- 112, "A Preliminary Cloudless Standard Atmosphere for Radiation Computation," IAMAP (International Association for Meteorology and Atmospheric Physics), Boulder, CO, pp.53, 1984.

[39] W. A. Abdou, J. V. Martonchik. R. A. Kahn, R. A, West, and D. J. Diner, "A modified linear-mixing method for calculating atmospheric path radiances of aerosol mixtures," *J. Geophys. Res.* **102, 16883-16888, 1997.**

[40] R. S. Fraser, "Satellite measurement of mass of Sahara dust in the atmosphere," *Appl. Opt. 15,2471-2479, 1976.*

[41] M. Griggs, "Measurements of atmospheric aerosol optical thickness over water using ERTS- 1 data," *J. Air Pollut. Control Assoc. 25,622-626, 1975.*

[42] M. Griggs, "Satellite measurements of tropospheric aerosols," *Adv. Space Res.* 2,109-118, 1983.

[43] C. S. Long and L. L. Stowe, "Using the NOAA/AVHRR to study stratospheric aerosol optical thickness following the Mt. Pinatubo eruption," *Geophys. Res. Lett.* **21,2215-2218, 1994.**

[44] L. L. Stowe, R. M. Carey, and P. P. Pellegrino, "Monitoring the Mt. Pinatubo aerosol layer with NOAA/1 1 AVHRR data," *Geophys. Res. Left. 19,* 159-162, 1992.

[45] M. A. Mishchenko, A. A. Lacis, B. E. Carlson, and L. D. Travis, "Nonsphericity of dust-like tropospheric aerosols: Implications for aerosol remote sensing and climate modeling," *Geophys. Res. Lett.* 22, 1077-1080, 1995.

[46] R. Kahn, R. West, D. McDonald, B. Rheingans, and M.] Mishchenko, "Sensitivity of multi-angle remote sensing observations to aerosol sphericity," *J. Geophys. Res.* 102, 16861-*16870,* 1997.

[47] R. Kahn, P. Banerjee, and D. McDonald, "Sensitivity of multiangle imaging to aerosol optical depth, and to pure-particle size distribution and composition over ocean," *J. Geophys. Res.*, in preparation, 1997.

[48] Y. J. Kaufman and C. Sendra, "Algorithm for atmospheric corrections," *Int. J. Remote Sens.* 9, 1357-1381, 1988.

[49] M. D. King, Y. J. Kaufman, W. P. Menzel, and D. Tanre, "Remote sensing of cloud,

aerosol, and water vapor properties from the Moderate resolution Imaging Spectrometer (MODIS)," *IEEE Trans. Geosci. Remote Sens. 30,2-27, 1992.*

[50] J. V. Martonchik, D. J. Diner, R. Kahn, T. P. Ackerman, M. M. Verstraete, B. Pin(y, and H. R. Gordon, "Techniques for the retrieval of aerosol properties over land and ocean using multi-angle imaging," *IEEE Trans. Geosci. Remote Sens.*, this issue, 1997.

[51] H. Rahman, H., B. Pinty, and M.M. Verstraete, "Coupled Surface-Atmosphere Reflectance (CSAR) model. 2. Semiempirical surface model usable with NOAA Advanced Very High Resolution Radiometer data," *J. Geophys. Res.* 98,20791-20801, 1993.

[52] J. V. Martonchik, "Determination of aerosol optical depth and land surface directional reflectance using multi-angle imaging," *J. Geophys. Res.* **102, 17015-17022, 1997.**

[53] R. E. Dickinson, "Land surface processes and climate-surface albedos and energy balance," *Adv. Geophys. 25, 305-353,* 1981.

[54] D. S. Kimes, P. J. Sellers and D. J. Diner, "Extraction of spectral hemispherical reflectance (albedo) of surfaces from nadir and directional reflectance data," *Int. J. Rem. Sens.* 8, 1727-1746, 1987.

[55] P. J. Sellers, "Canopy reflectance, photosynthesis and transpiration," *Int. J. Rem. Sens.* 6, 1335-1372, 1985.

[56] P. J. Sellers, "Canopy reflectance, photosynthesis and transpiration 11: The role of biophysics in the linearity of their interdependence," *Rem. Sens. Env.* **21, 143-183, 1987.**

[57] F. G. Hall, D. E. Strebel, S. J. Goetz, K. D. Woods and D. B. Botkin, "Landscape pattern and successional dynamics in the boreal forest," *Proceedings of the 1987 IGARSS Symposium,* **IEEE 87 CH2434-9**, *473, 1987.*

[58] S. A. W. Gerstl and C. Simmer, "Radiation physics and modeling for off-nadir satellite-sensing of non-l am bertian surfaces." *Rem. Sens. Environ. 20,* 1*-29, 1986.*

[59] D. S. Kimes and P. J. Sellers, "Inferring hemispherical reflectance of the Earth's sur-

face for global energy budgets from remotely sensed nadir or directional radiance values," *Rem. Sens. Environ, 18,205-223, 1985.*

[60] N. Gobron, B. Pinty, M. M. Verstraete, R. B. Myneni, J. V. Martonchik, Y. Knyazikhin, and D. J. Diner, "The potential of multi-angular spectral measurements to characterize land surfaces: Conceptual approach, and exploratory application," *IEEE Trans. Geosci. Remote Sens.,* this issue, 1997.

[61] C. S. Potter, J. T. Randerson, C. B. Field, P. A. Matson, P. M. Vitousek, H. A. Mooney, and S. A. Klooster, "Terrestrial ecosystem production: A process model based on global satellite and surface data," *Global Biogeochem. Cycles 7, 811-841,* 1993.

[62] S. D. Prince, "A model of regional primary production for use with coarse resolution satellite data," in?. *J. Rem. Sens. 12, 1313-1330,* 1991.

[63] S. W. Running and J. C. CoughIan, "A general model of forest ecosystem processes for regional applications, I, Hydrological balance, canopy gas exchange and primary production processes," *Ecol. Model. 42,* 125-154, 1988.

[64] J. V. Martonchik, D. J. Diner, B. Pinty, M. M. Verstraete, R. Myneni, Y. Knyazikhin, and H. R. Gordon, "Determination of land and ocean reflective, radiative, and biophysical properties using multi-angle imaging," *IEEE Trans. Geosci. Remote Sens.*, this issue, 1997.

[65] H. R. Gordon, D. K. Clark, J. W. Brown, O. B. Brown, R. H. Evans and W. W. Broenkow, "Phytoplankton pigment concentrations in the Middle Atlantic Bight: Comparison of ship determinations and Coastal Zone Color Scanner measurements," *Appl. Opt. 22, 20-36, 1983.*

AUTHOR BIOGRAPHIES

David J. Diner received the B.S. degree in physics with honors from the State University of New York at Stony Brook in 1973 and the M.S. and Ph.D. degrees in planetary science from the California Institute of Technology in 1977 and 1978, respectively. He has been at the Jet Propulsion Laboratory since 1978, first as a National Research Council Resident Research Associate, then as a contractor with Ball Aerospace, and since 1981 as a JPL employee. He is currently a Member of the Technical Staff and Leader of the Multi-angle Imaging Science Element in the Earth and Space Sciences Division. He has been involved in numerous NASA planetary and Earth remote-sensing investigations, and is presently Principal Investigator of the EOS Multi-angle Imaging SpectroRadiometer (MISR) experiment and its airborne counterpart, AirMISR.

Jewel C. Beckert has been employed at the Jet Propulsion Laboratory for forty years. During that time he has participated in most of the planetary missions carried out by the laboratory, concentrating on assembly, test, and launch of spacecraft. In the 1980's he contributed to the Hubble Space Telescope as Deputy Manager of the Wide Field/Planetary Camera (WFPC) 1 and 2 Projects. He is presently Deputy Manager and Instrument Manager for the MISR Project.

Terrence H. Reilly received the Ph.D. degree in physics from the Institute of Optics at the University of Rochester in 1969. He joined JPL that same year, and held various assignments in the Mariner Venus/Mercury, Viking, and Voyager projects. He was later appointed supervisor of the group responsible for optics and focal plane detectors for the Wide Field/Planetary Camera on the Hubble Space Telescope. In 1985-86 he was a supervisor in the Government Systems Division at Eastman Kodak, but later returned to JPL. In recent years he was Instrument Manager for the imaging instruments on the Comet Rendezvous/Asteroid Flyby and Cassini projects. Since 1992, he has been Manager of the MISR Project.

Carol J. Bruegge received the B.A. and M.S. degrees in applied physics from the University of California at San Diego in 1978 and the M.S. and Ph.D. degrees in optical sciences from the University of Arizona in 1985. She joined JPL in 1985, where she is presently a Member of the Technical Staff. Her experience is principally in the areas of terrestrial remote sensing, radiative

transfer, instrument calibration, and the application of ground-truth measurements to the radiometric calibration of remote sensing instruments, such as the Landsat Thematic Mapper, the Airborne Imaging Spectrometer (AIS), and the Airborne Visible/Infrared Imaging Spectrometer (AVIRIS). She has participated in the First International Land Surface Climatology Program Field Experiment (FIFE) as a Principal Investigator. Dr. Bruegge is presently the Instrument Scientist for MISR, for which she oversees the pre-flight and in-flight radiometric calibration and characterization efforts and coordinates the activities of the MISR calibration and validation teams.

James E. Conel received the B.A. degree in geology from Occidental College in 1955, the M.S. and Ph.D. degrees from the California Institute of Technology, in geology, in 1957 and 1962. He has been at the Jet Propulsion Laboratory since 1962 and has participated as Principal Investigator in numerous investigations involving lunar geology, reflectance, thermal emission spectroscopy and geophysics, application of multispectral remote sensing methods to exploration for uranium deposits, mapping of Pleistocene/Quaternary and modern river terraces in Wyoming to determine response of the Earth's crust to isostatic rebound from erosion and as response to Yellowstone hotspot motion. Currently he is a Member of the Technical Staff at JPL and is the Validation Scientist for MISR.

Ralph A. Kahn received his Ph.D. in applied physics from Harvard University in 1980, concentrating in atmospheric physics and radiative transfer. His research interests include the climate and climate history of Mars, Venus, and Earth. A primary theme of his work has been to analyze global-scale data sets, bringing to bear theoretical models and other observations as needed. He was an experimenter on the Viking Lander Imaging team, and was responsible for imaging the sunset of Mars. He has been a Research Scientist at the Jet Propulsion Laboratory since 1988, where he works primarily on Earth observations. He is a member of the MISR science team, specializing in tropospheric aerosol research. Dr. Kahn has lectured on global change and atmospheric physics at UCLA, the Claremont Colleges, and Caltech, and is editor and founder of PUMAS, the on-line journal of science and math examples for pre-college education (http://pumas.jpl.nasa.gov).

John V. Martonchik received the B.S. degree in physics from Case Institute of Technology in 1964 and the Ph.D. degree in astronomy from the University of Texas at Austin in 1974. He joined

JPL in 1972 and currently holds the position of Research Scientist. His experiences include telescopic and spacecraft observations of planetary atmospheres, laboratory and theoretical studies of the optics] properties of gaseous, liquid, and solid materials, and development and implementation of one- and three-dimensional radiative transfer and line-by-line spectroscopy algorithms for studies of planetary atmospheres and Earth tropospheric remote sensing. He has been a Co-Investigator in several NASA programs and is the Algorithm Scientist for aerosol and surface retrievals on MISR.

Thomas P. Ackerman received the M. SC. degree in physics in 1971 and the Ph.D. in atmospheric science in 1976 from the University of Washington. He has been a member of the faculty at the Pennsylvania State University since 1988 and holds the positions of Professor of Meteorology and Associate Director of the Earth System Science Center. Prior to 1988, he was a research scientist at the NASA Ames Research Center. His research interests include radiative transfer in planetary atmospheres, the effect of aerosol and clouds on the Earth radiation budget, and remote sensing of aerosol and cloud properties both from ground and satellite. He is currently a member of the MISR science team and Site Scientist for the Tropical Western Pacific site in the DOE Atmospheric Radiation Measurement Program.

Roger Davies received the B.Sc degree with honors in physics from Victoria University of Wellington, New Zealand in 1970 and the Ph.D. in meteorology from the University of Wisconsin-Madison in 1976. He joined the faculty of the University of Arizona, Tucson, as an associate professor of atmospheric science in 1995, and was formerly on the faculties of Purdue University, West Lafayette, Indiana and McGill University, Montreal, Canada. He teaches courses on Atmospheric Physics, Radiation, and Climate Theory and directs a laboratory on applications of radiative transfer to remote sensing. His main area of current research is the interaction of cloud heterogeneity with atmospheric radiation. Dr. Davies is a member of the MISR science team and a member of the International Radiation Commission.

Siegfried A.W. Gerstl has been a scientific staff member at the Los Alamos National Laboratory since 1974 and is presently a project leader for remote sensing science. He holds a Ph.D. in physics from the [University of Karlsruhe, Germany, and an M.S. and B.S. in mathematics and chemistry, and has published over 50 full-length scientific papers in refereed journals. His primary interests

and expertise are in science and technology related to satellite remote sensing and analysis, with emphasis on modeling and data interpretation. Current fields of special interest are the theory and application of radiative transfer and radiosity methods, atmospheric corrections, angular and spectral signatures in active and passive remote sensing, and the development of new satellite and sensor concepts. Dr. Gerstl is an active scientific investigator in NASA's Earth Observing System (EOS) and a MISR science team member.

Howard R. Gordon is Professor of Physics at the University of Miami. He received the B.S. degree in physics from Clarkson College of Technology (now Clarkson University) in 1961 and the M.S. and Ph.D. degrees in physics from the Pennsylvania State University in 1963 and 1965, respectively. In 1975 he became a member of the Nimbus-7 Coastal Zone Color Scanner (CZCS) experiment team --- the first satellite instrument designed to study the variability in the distribution of phytoplankton in the ocean. He was awarded the Public Service Medal by NASA in 1982 for the development of methods for recovering phytoplankton pigment concentrations from CZCS imagery. He is presently a science team member of a number of new satellite instruments designed for a long-term assessment of global climate: the Sea-viewing Wide-Field-of-View Sensor (SeaWiFS), a CZCS follow-on to globally monitor the concentration of marine phytoplankton, launched August 1, 1997; the Moderate Resolution Imaging Spectroradiometer (MODIS) to be launched in 1998; and the Multi-angle Imaging SpectroRadiometer (MISR) to be launched in 1998. He was elected Fellow of the Optical Society of America in 1977, and has served as the Oceanic Optics Topical Editor of Applied Optics.

Jan-Peter A. L. Muller received a B. SC. degree in Physics with honours from Sheffield University in 1976, an M. SC. in Atmospheric Physics and Dynamics from Imperial College London in 1977 and a Ph.D. in Planetary Meteorology from University College London in 1982. He is currently a full professor in the Department of Geomatic Engineering at University College London, UK. He is a member of the MISR and MODIS science teams on EOS and a Co-Investigator on the European POLDER, VEGETATION, and ATSR-2 instruments. His research interests include the development and application of automated image understanding algorithms and systems to global environmental monitoring from space and the visualization of global change.

Ranga B. Myneni obtained his Ph.D. in Biology from the University of Antwerp in Belgium in

1985. Since then, he has worked at Kansas State, the University of Gottingen and NASA Goddard Space Flight Center. He is now an Associate Professor in the department of Geography at Boston University. His research interests are radiative transfer, remote sensing of vegetation and climate-vegetation dynamics. He is a member of the MODIS and MISR science teams.

Piers J. Sellers received the B. SC. degree in ecological science from the University of Edinburgh (Scotland) in 1976, and received a doctorate in biometeorology from Leeds University (United Kingdom) in 1981. In 1982 he became a National Research Council Resident Research Associate at Goddard Space Flight Center working on surface energy balance computer models and in 1984 became a Faculty Research Scientist at the University of Maryland. He received the Arthur Fleming Award in 1995 and the American Meteorology Society Houghton Award in 1997. He has been involved in computer modeling of the climate system, satellite remote sensing studies, and coordinated field work utilizing aircraft, satellites, and ground teams in Kansas, Russia, Africa, Canada and Brazil, and is a member of the MISR science team. Dr. Sellers was selected as an astronaut candidate by NASA in 1996 and reported to the Johnson Space Center to begin two years of training and evaluation. Successful completion of initial training will qualify him for various technical assignments leading to selection as a Mission Specialist on a Space Shuttle flight crew.

Bernard Pinty received his Maîtrise de Chimie and DEA (1977), thèse de troisième cycle en Physique de I'Atmosphere (1980) and thèse d'Etat (1988) from the Université Blaise Pascal in Clermont-Ferrand, France. He is presently affiliated with the Space Applications Institute (SAI) in Ispra, Italy. He visited the National Center for Atmospheric Research (NCAR) in Boulder, CO (1988- 1989), served as Deputy Director of the Laboratoire d'Etudes et de Recherches en Télédétection Spatiale (LERTS) in Toulouse, France (1990- 1992), and was Professor of Physics at the University Blaise Pascal, France (1993- 1996). Dr. Pinty received the Zel'dovich medal from COSPAR (1990) and is a member of the MERIS Scientific Advisory Group of the European Space Agency and a MISR science team member. He serves as an Associate Editor for the Journal of Geophysical Research-Atmosphere. His main interests include research on the theory of radiation transfer in plant canopies and, more generally, the development of tools to quantitatively interpret satellite remote sensing data in the solar spectral domain.

Michel M. Verstraete received his License en Physique (1974) from the Université Catholique de Louvain in Louvain-la-Nueve, Belgium, his License Spéciale en Géophysique (1976) from the Université Libre de Bruxelles, Belgium, and both his M. SC. in Meteorology (1978) and D. SC. in Atmospheric Sciences (1985) from the Massachusetts Institute of Technology in Cambridge, MA. He worked for the World Meteorological Organization in Geneva, Switzerland and Nairobi, Kenya from 1979-1981, at the National Center for Atmospheric Research (NCAR) in Boulder, CO from 1982-1989, taught at the University of Michigan in Ann Arbor from 1989-1990, and is currently employed at the Space Applications Institute (SAI) in Ispra, Italy. He is a member of various scientific advisory committees of the European Space Agency (e.g., MERIS) and is a MISR science team member. His initial work on topics such as the modeling of atmosphere-biosphere interactions and desertification led him to his current interest in the quantitative exploitation of satellite remote sensing data for the detection and characterization of terrestrial surface properties.

FIGURE CAPTIONS

Figure 1

This graphic illustrates the measurement approach of the MISR instrument. Nine pushbroom cameras point at discrete angles along the spacecraft ground track, and data in four spectral bands are obtained for each camera. It takes 7 minutes for a point on the Earth to be observed at all nine angles.

Figure 2

This is an artist's rendition of the MISR instrument in cutaway view. The back ends of the 9 MISR cameras appear as cylinders. In this orientation, MISR would look down toward the Earth.

Figure 3

The MISR instrument is shown seated on the end bell of the thermal vacuum chamber in the 10-foot Space Simulator Facility at the Jet Propulsion Laboratory. Testing within this chamber was used to verify the instrument performance over a range of temperatures.

Figure 4

Conceptual flow of MISR data through the product generation system.

TABLE CAPTIONS

Table I

MISR instrument system requirements and as-built specifications.

Table II

MISR camera pointing requirements and as-built specifications.

Table III

MISR radiometric and spectral requirements and as-built specifications.

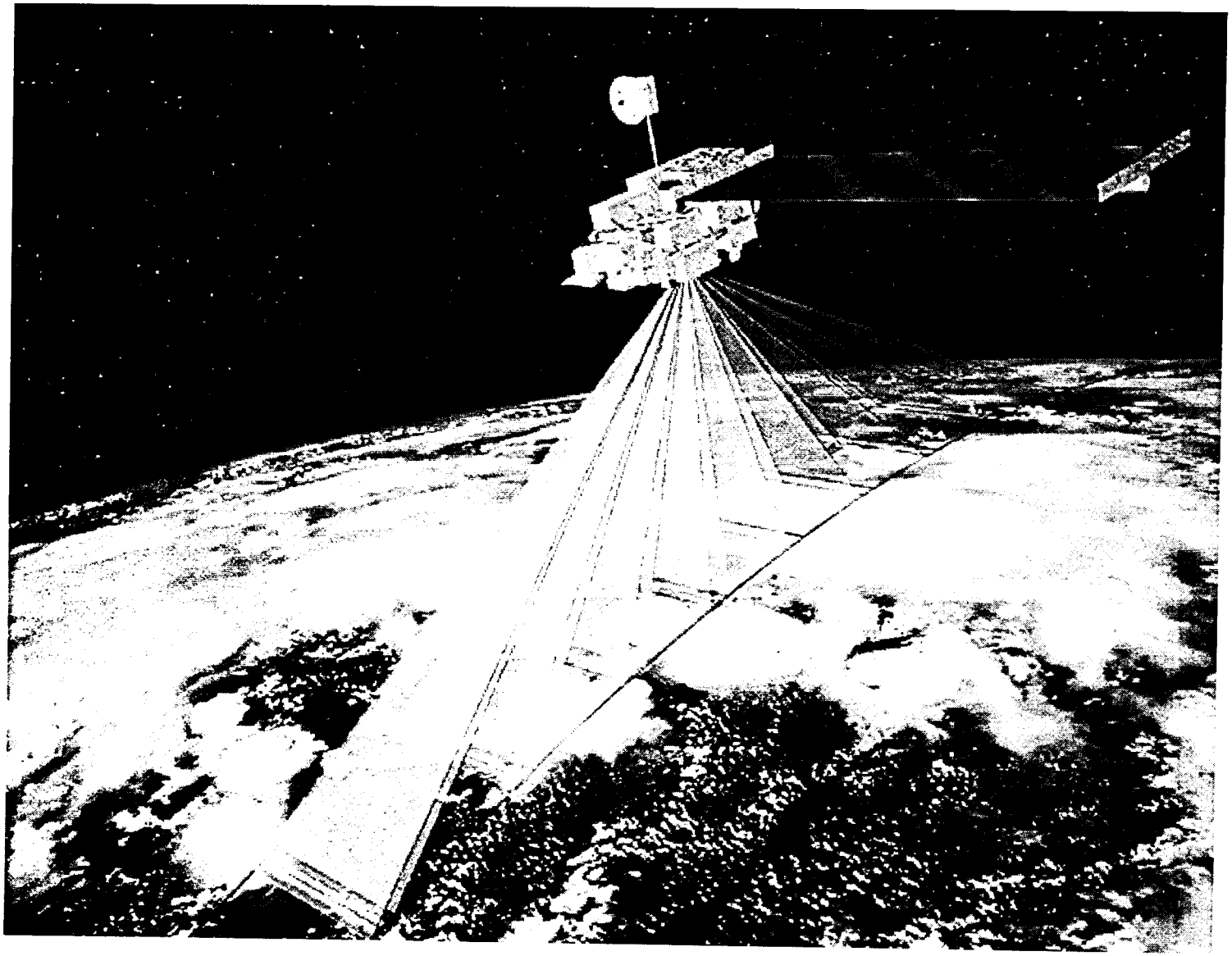

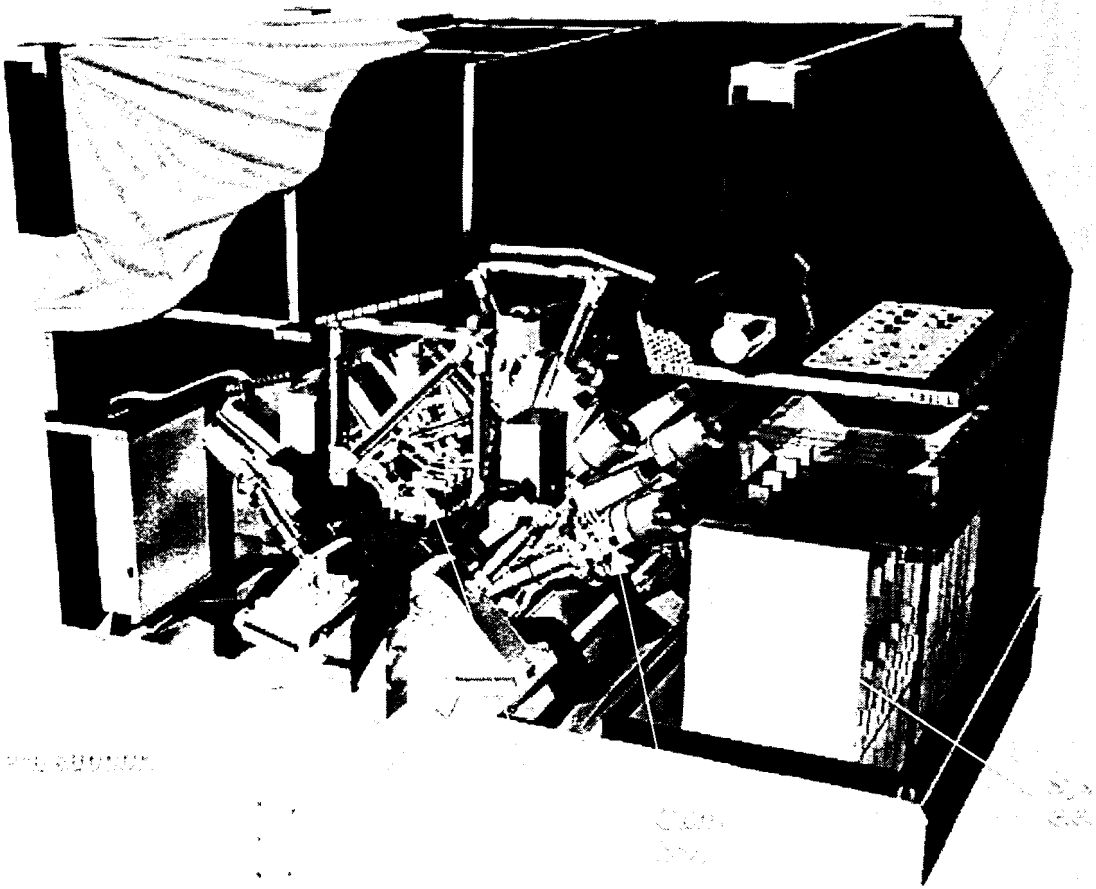

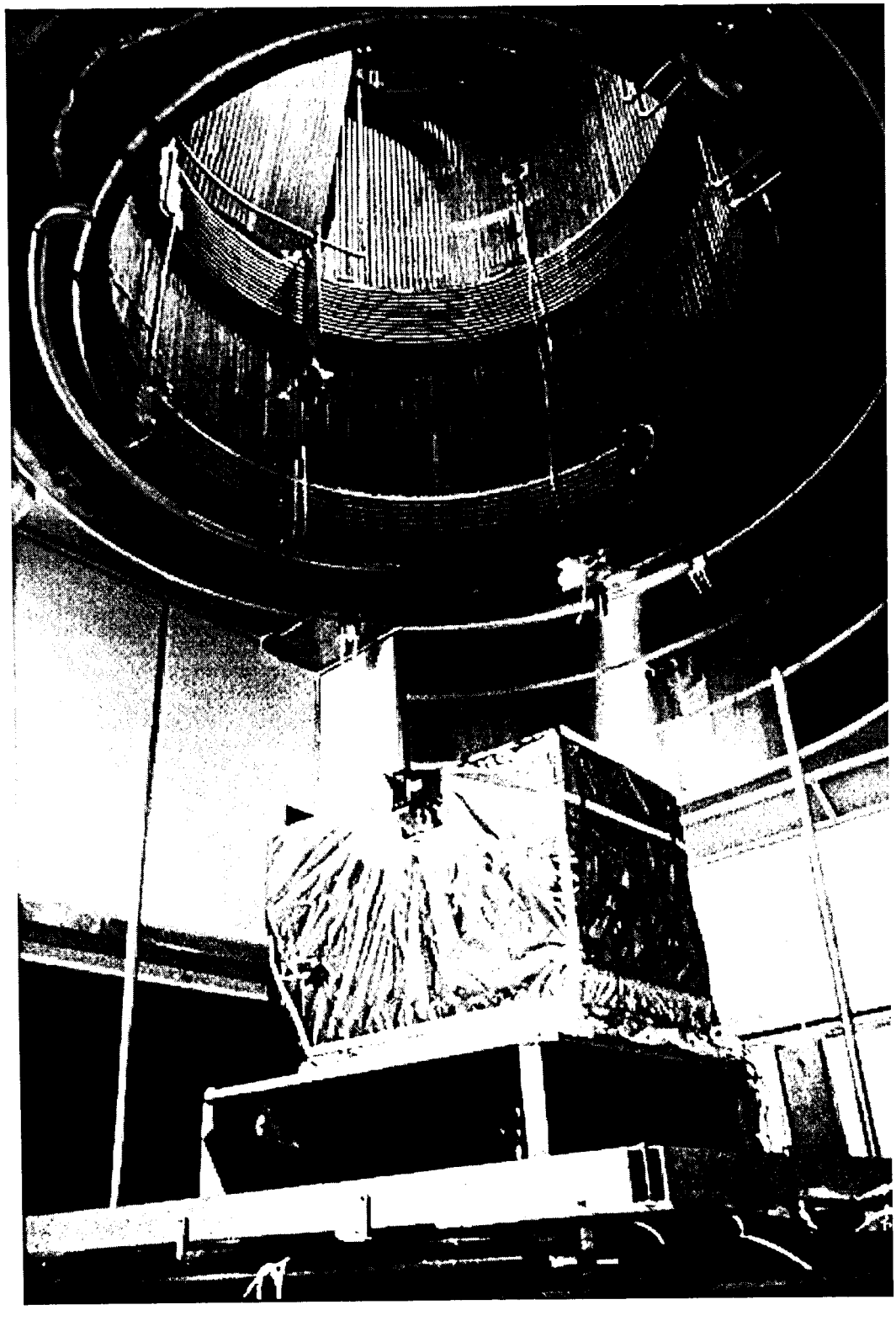

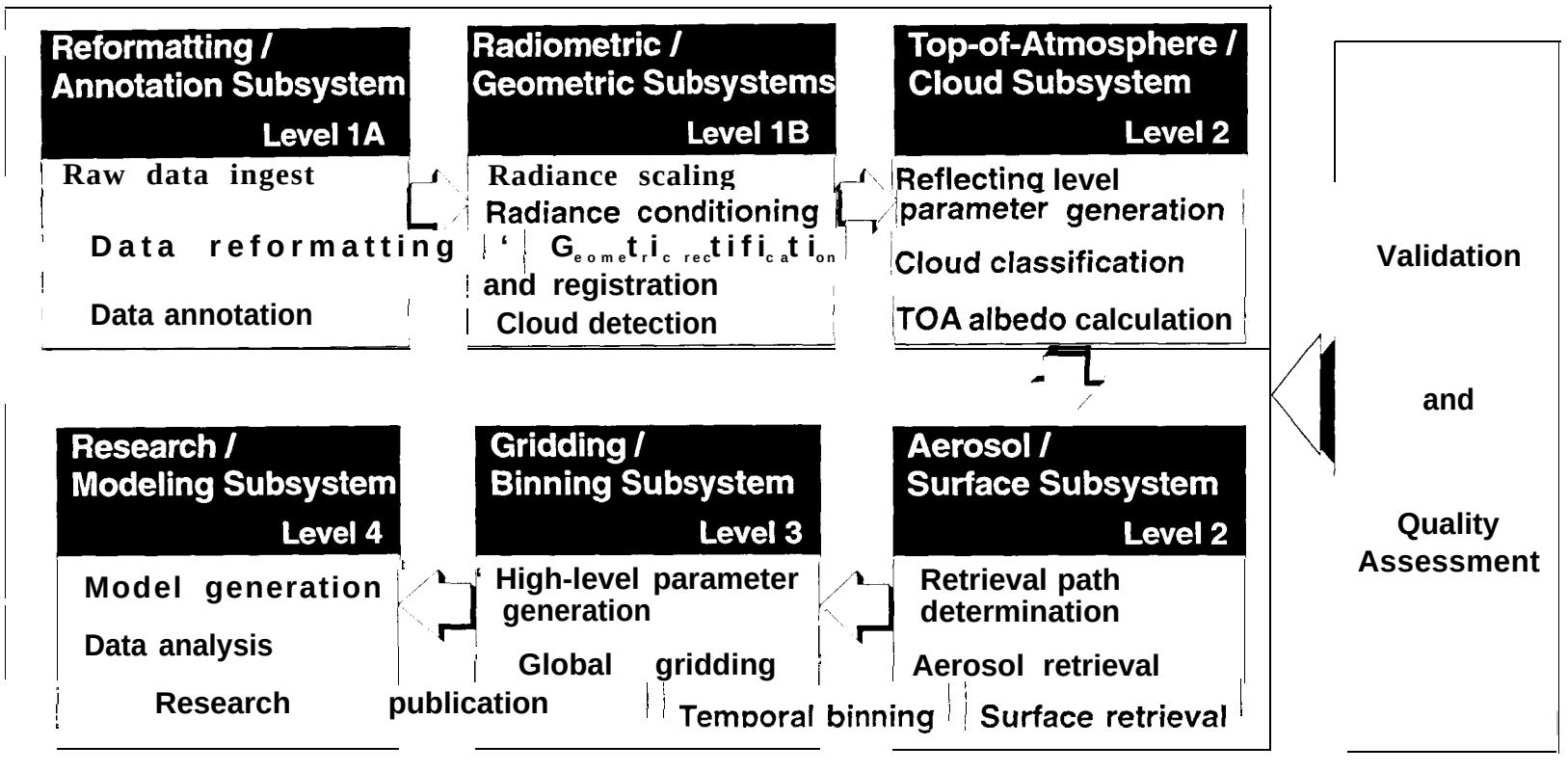
Reformatting / Annotation Subsystem
Level 1A
Raw data ingest
Data reformatting
Data annotation
Radiometric / Geometric Subsystems
Level 1B
Radiance scaling
Radiance conditioning
Geometric rectification
and registration
Cloud detection
Top-of-Atmosphere / Cloud Subsystem
Level 2
Reflecting level parameter generation
Cloud classification
TOA albedo calculation
Validation
and
Quality Assessment
Research / Modeling Subsystem
Level 4
Model generation
Data analysis
Research publication
Gridding / Binning Subsystem
Level 3
High-level parameter generation
Global gridding
Temporal binning
Aerosol / Surface Subsystem
Level 2
Retrieval path determination
Aerosol retrieval
Surface retrieval

Table I

Parameter	Specification	As-Built
Size	Specified by spacecraft envelope	**0.9** m (W) x 0.9 m (H) x 1.3 m (L)
Mass	≤ 157 kg	149 kg
Power	≤ 77 W (worst case orbital average) ≤ 130W (peak)	S3 W (worst case orbits! average) 131 W (peak)
Data Rate (orbital average)	≤3.8 Mbps	3.3 Mbps
Quantization	Established by signal-to-noise ratio requirements	14 bits linear, compressed by square-root encoding to 12 bits
Spatial Sampling	! 275 m. 550 m. or 1.1 km (individually commendable for each channel)	As specified
Swath width (minimum overlap at all nine view angles along a line of constant latitude)	360 km	389 km

Table II

Camera	View angle		Boresight angle		Swath offset angle		Effective focal length (mm)	
	Specification	As-Built	Specification	As-Built	Specification	As-Built	Specification	As-Built
if	70.5° (forward)	70.3°	**58.0** ± 0.2°	57.88°	**-2.7 ± 0.2°**	-2.62°	123.8 ± 1.9	123.67
Cf	60.0° (forward)	60.2°	51.2 ± 0.2°	51.30’	-2.3 ± 0.2°	-2.22°	95.3 ± 1.4	95.34
Bf	45.6° (forward)	45.7°	40.0 ± 0.2°	40.10°	-1.7 ± 0.2°	-1.71°	73.4 ± 1.1	73.03
Af	26.1° (forward)	26.2°	23.3 ± 0.2°	23.34”	**-1.0** ± 0.2°	-1.06°	59.3 ± 0.9	58.90
An	**0.0** ° (nadir)	0.1°	0.0 ± 0.2°	-0.04°	0.0* 0.2°	0.04°	59.3 ± 0.9	58.94
Aa	26.1 (aftward)	26.2°	-23.3 ± 0.2°	-23.35°	1.0 ± 0.2°	1.09°	59.3* 0.9	59.03
Ba	45.6° (aftward)	45.7°	-40.0 ± 0.2°	-40.06°	1.7 ± 0.2°	1.76°	73.4 ± 0.9	73.00
Ca	60.0” (aftward)	60.2°	-51.2 ± 0.2°	-51.31°	2.3 ± 0.2°	2.24°	95.3 ± 1.4	95.33
Da	70.5° (aftward)	70.6°	-58.0 ± 0.2°	-58.03°	2.7 ± 0.2°	2.69°	123.8 ± 1.9	123.66

View publication stats

Table III

Parameter	Specification	As-Built
Spectral Bands (solar weighted, measured in-band response)	Blue: 443 ± 2 nm Green: 555 ± 2 nm Red: 670 ± 2 nm NearIR: 865 ± 2 nm	Blue: 446.4 nm Green: 557.5 nm Red: 671.7 nm NearIR: 866.4 nm
Spectral Bandwidths (solar weighted, measured in-band response)	Blue: ≤ 30 nm Green: ≤ 20 nm Red: ≤ 20 nm NearIR: ≤ 60 nm	Blue: 41.9 nm Green: 28.6 nm Red: 21.9 nm NearIR: 39.7 nm
Polarization Sensitivity	≤ 1%	As specified
Absolute Radiometric Uncertainty	≤ 3% of absolute radiance at full signal	2%
Signal-to-Noise Ratio	≥ 700 at full signal at highest spatial resolution	As specified